Applied Catalysis B: Environmental 162 (2015) 141–148

Contents lists available at ScienceDirect

Applied Catalysis B: Environmental

journal homepage: www.elsevier.com/locate/apcatb

New insights into reaction mechanisms of ethanol steam reforming on Co–ZrO_2

Junming Sun[a], Ayman M. Karim[b], Donghai Mei[b], Mark Engelhard[b], Xinhe Bao[c], Yong Wang[a,b,*]

[a] The Gene & Linda Voiland School of Chemical Engineering and Bioengineering, Washington State University, Pullman, WA 99164, USA
[b] Institute for Integrated Catalysis, Pacific Northwest National Laboratory, Richland, WA 99352, USA
[c] State Key Laboratory of Catalysis, Dalian Institute of Chemical Physics, Chinese Academy of Science, China

ARTICLE INFO

Article history:
Received 23 March 2014
Received in revised form 3 June 2014
Accepted 24 June 2014
Available online 1 July 2014

Keywords:
Ethanol steam reforming
Cobalt
Reaction pathway
Acetone
Oxidation state

ABSTRACT

The reaction pathway of ethanol steam reforming on Co–ZrO_2 has been identified and the active sites associated with each step are proposed. Ethanol is converted into acetaldehyde and then into acetone, followed by acetone steam reforming. More than 90% of carbon was found to follow this reaction pathway. N_2 sorption, X-ray diffraction (XRD), temperature-programmed reduction (TPR), in situ X-ray photoelectron spectroscopy (XPS), transmission electron microscopy, as well as theoretical density functional theory (DFT) calculations have been employed to identify the structure and functionality of the catalysts, which was further used to correlate their performance in ethanol steam reforming (ESR). It was found that metallic cobalt is mainly responsible for the acetone steam-reforming reactions, while CoO and basic sites on the support play a key role in converting ethanol into acetone via dehydrogenation and condensation/ketonization reaction pathways. The current work provides fundamental understanding of the ethanol steam-reforming reaction mechanisms on Co–ZrO_2 catalysts and sheds light on the rational design of selective and durable ethanol steam-reforming catalysts.

1. Introduction

Due to its low carbon footprint and renewable source, steam reforming of biomass-derived ethanol (ESR) has been extensively investigated to produce hydrogen for hydrotreating of biomass-derived oxygenates or the potential fuel-cell application [1]. Previous experimental studies on ethanol steam reforming (ESR) over a number of supported metal catalysts suggested that the catalytic performance largely depends on the operating conditions, the nature of metal as well as the supports [2–21], which have also been summarized in a few recent reviews [22–28].

Among the metals studied, noble metal catalysts exhibited high methane selectivity and low hydrogen yield at low temperatures (<500 °C) [17,22,24], whereas cobalt-based catalysts was found promising for its low-cost, low methane selectivity and high selectivity to hydrogen [2,4,25]. Numerous studies have shown that support exerted a very complicated effect on both water dissociation [29] and cobalt oxidation states in ESR [25,26]. For example, metal oxide support (e.g., CeO_2, ZnO–CeO_2 and CeO_2–ZrO_2) was found to be essential to the water dissociation and thus oxygen supply for removing the carbonaceous species (e.g., CH_x) on the catalysts in ESR [11,12]. However, this effect of support was also found to facilitate the oxidation of cobalt that led to decreased C–C cleavage activity [30], depending on the composition of the reaction stream [14], the pretreatment and the composition of catalysts [16,30–32]. On the other hand, due to the lack of active site for water dissociation, inert carbon-supported Co nanoparticles (i.e., Co/g-AC) was found resistant to oxidation by water under the ESR conditions [33]. Interestingly, cobalt particles at nanoscale (i.e., 5 nm) was favorite for the water dissociation even in the absence of metal oxides, gasification of CH_x species and steam-reforming activity was thus maintained on the inert carbon-supported cobalt nanoparticles [33]. In this case, metal oxide-catalyzed condensation and oligomerization of acetone [34,35] was able to be avoided, and coking reaction was thus alleviated on the Co/g-AC catalysts during steam reforming [33].

The effects of oxidation state of cobalt as well as support on the reaction network have been widely investigated in ESR [6,7,36].

* Corresponding author at: The Gene & Linda Voiland School of Chemical Engineering and Bioengineering, Washington State University, Pullman, WA 99164, USA.
E-mail address: yong.wang@pnnl.gov (Y. Wang).

http://dx.doi.org/10.1016/j.apcatb.2014.06.043
0926-3373/

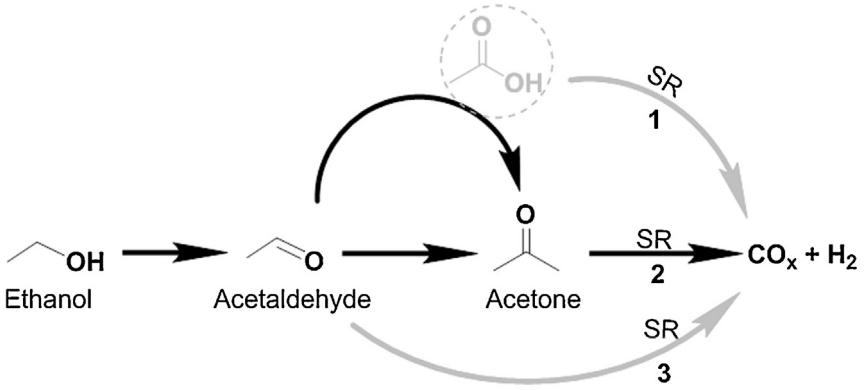

Scheme 1. Proposed main reaction pathway for ethanol steam reforming on cobalt-based catalysts (SR = steam reforming).

Both Co^{2+} and Co^0 have been found to be active for ethanol dehydrogenation to acetaldehyde [36] while Co^0 is highly active for C–C bond cleavage [16,32]. Cobalt supported on the basic metal oxides (e.g., ZnO, CeO_2, ZrO_2) has shown high activity and selectivity in ESR [7,8,12,37]. Over Co/ZnO, Llorca et al. [18] proposed a major reaction pathway from ethanol to acetaldehyde, followed by direct acetaldehyde steam-reforming reactions (Scheme 1, path 3) or acetaldehyde steam reforming via acetic acid intermediate (Scheme 1, path 1). Later, a similar reaction pathway was confirmed on the Co/ZrO_2 catalysts by Song et al. [11,12]. It should be mentioned that acetone was formed on these basic metal oxide-supported cobalt catalysts, but has been routinely identified as an undesired intermediate that causes the coking and deactivation of catalysts [6,8,12,35,38–41]. Recently, we found that acetone may be a desired intermediate and acetone steam reforming can readily take place on cobalt nanoparticles to selectively produce hydrogen [33]. The facile C—H bond cleavage relative to the C—C bond scission of acetone combined with the facile water dissociation and oxidation of CH_x* lead to very high selectivity and stability of the cobalt nanoparticles catalysts for acetone steam-reforming reactions. In this work, based on a systematic investigation of ESR over Co–ZrO_2, we show that acetone acts as the major reaction intermediate which is steam reformed selectively to H_2 and CO_2 on metallic cobalt nanoparticles at 450 °C. In this sequential reaction pathway, cobalt is found to play a bifunctional role in transforming ethanol to H_2 and CO_2 with high selectivity. Non-reducible cobalt (cobalt species strongly interacted with ZrO_2 support) passivates most of the strong acidic sites on ZrO_2 and suppresses the undesired dehydration of ethanol on the support. In the meantime, dehydrogenation and condensation/ketonization reaction pathway is enhanced, resulting in the acetone formation. Metallic cobalt nanoparticles attached on the tips of carbon nanotube (Co/CNF, from reducible cobalt) developed during the ESR was found to be mainly responsible for the following acetone steam reforming reactions.

2. Experimental

2.1. Materials and synthesis

Cobalt nitrate hexahydrate (≥98%), ethanol (200 proof), acetaldehyde (≥99.5%) and acetone (≥99.9%) were purchased from Sigma–Aldrich. ZrO_2 support was obtained by calcining $Zr(OH)_4$ (FZO/935) at 600 °C for 3 h in air. All the Co–ZrO_2 catalysts were prepared by impregnation of ZrO_2 with aqueous solutions of cobalt nitrate hexahydrate followed by drying at 100 °C for 3 h. The powder samples were then calcined at 550 °C for 5 h (ramping rate, 5 °C/min) in air to get as-synthesized catalysts. The cobalt loading amount was varied between 2 and 10 wt% by controlling the concentration of cobalt precursor. 8 wt% Co/CNF (CNF represents carbon nanofilaments) catalysts (8Co–CNF) were prepared according to an established procedure [42]. The details regarding catalysts preparation, notion and physical/chemical properties are summarized in Table 1.

2.2. Characterization

XRD patterns were collected on a Philips X'pert MPD (Model PW 3040/00) equipped with a Cu Kα X-ray source operating at 40 kV and 50 mA. Nitrogen adsorption–desorption isotherms were recorded on a Micromeritics (Tristar 3000) apparatus. Before adsorption analysis, samples were degassed at 250 °C for 2 h. H_2 Temperature-programmed reduction (H_2-TPR) profile was collected on a Micromeritics Autochem II 2920 system. Briefly, 100 mg samples were packed into a U-shaped reactor, and ramped to 600 °C at 10 °C/min under flowing 5% H_2/Ar. TEM images were recorded on a JEOL-2010 transmission electron microscope. In situ X-ray photoelectron spectroscopy (XPS) measurements were performed using a Physical Electronics Quantum 2000 Scanning ESCA Microprobe. This system uses a focused monochromatic Al Kα X-rays (1486.7 eV) source and a spherical section analyzer. The instrument

Table 1
Catalysts notation and physical/chemical parameters.

Catalysts	Notion	BET surface area (m^2/g)	$Co^0/(Co^0 + Co^{x+})$ (%)[a] (Co^0/Co^{2+} ratio)	
			Reduced	Reduced then exposed to H_2O
ZrO_2	ZrO_2	62.1	–	–
2 wt% Co/ZrO_2	2Co–ZrO_2	58.4	14.4 (0.17)	1.4 (0.01)
5 wt% Co/ZrO_2	5Co–ZrO_2	51.2	30.3 (0.43)	8.9 (0.10)
10 wt% Co/ZrO_2	10Co–ZrO_2	46.0	69.3 (2.26)	40.1 (0.67)

[a] Calculated based on the in situ XPS measurement (see details in Section 2).

has a 16-element multichannel detector. The X-ray beam used was a 100 W, 100 μm diameter beam that was rastered over a 1.3 mm by 0.2 mm rectangle on the sample. The X-ray beam is incident normal to the sample and the photoelectron detector was at 45° off-normal. Wide scan data were collected using a pass energy of 117.4 eV. For the Ag $3d_{5/2}$ line, these conditions produce full-width half-maximum (FWHM) of better than 1.6 eV. The high-energy resolution photoemission spectra were collected using a pass energy of 46.95 eV. For the Ag $3d_{5/2}$ line, these conditions produced FWHM of better than 0.98 eV. The binding energy (BE) scale is calibrated using the Cu $2p_{3/2}$ feature at 932.62 ± 0.05 eV and Au 4f at 83.96 ± 0.05 eV for known standards. The sample experienced variable degrees of charging. Low-energy electrons at ca. 1 eV, 20 μA and low-energy Ar^+ ions were used to minimize this charging.

Before XPS measurement, the as-synthesized catalysts were reduced a 10% H_2/N_2 flow (50 STP ml/min) at 450 °C (ramping rate was 5 °C/min) for 2 h in a special designed chamber [16], followed by a 30 min purging with flowing He at same temperature. The reduced catalysts were cooled down under flowing He and then evacuated and transferred into the high-vacuum chamber for XPS measurement. For the H_2O-treated samples, the reduced catalysts were treated in flowing 3% H_2O/He at 450 °C for 30 min, followed by purging in flowing He for 30 min to remove the physisorbed H_2O, and then cool down for XPS experiments. We used a semi-quantitative empirical approach for fitting the XPS Co 2p peaks to estimate the fraction of Co (0) and Co^{2+} in the fresh supported cobalt samples as described previously [16].

2.3. Activity test

Ethanol steam reforming (ESR) reactions were conducted in a fixed-bed stainless steel reactor (i.d. 5 mm), which has been described elsewhere [33,43]. Typically, 100 mg of samples diluted with SiC dilutes (dilution ratio was 10) was packed and sandwiched by two quartz wool beds. The thermocouple was placed at the middle part of the catalyst bed to monitor the temperature. Before the reaction, catalysts were reduced in a 10% H_2/N_2 flow (50 STP ml/min) at 450 °C (ramping rate was 5 °C/min) for 2 h (catalysts at this stage are called fresh catalyst in the current paper) and then the reducing gas was switched to pure N_2 to purge the reaction system until no hydrogen was detected. After which, a mixture of ethanol/H_2O (steam/carbon ratio, S/C = 5) was injected into the vaporizer (180 °C) by a syringe pump (Core-Parmer WU-74900-00), and then carried into the reactor and through the catalyst bed by flowing nitrogen gas. The flow rate of N_2 and ethanol/H_2O mixture (steam to carbon ratio = 5) were adjusted to vary the residence time (W/F, g. s. ml^{-1}), while keeping the ethanol partial pressure constant at 7.2 kPa or as noted. The tube downstream before the cold trap was heated at 150 °C to avoid the condensation of liquid products. A Shimadzu 2014 GC, equipped with an auto sampling valve, HP-Plot Q column and FID detector, was placed between the reactor outlet and cold trap to collect and analyze the organic products in effluent gas. After the cold trap, the dry gas was sent to an online micro GC (MicroGC 3000A equipped with molecular sieves 5A, plot U columns and Thermal Conductivity Detectors (TCDs)) for the analysis of small organic and inorganic gases (e.g., CH_4 ethylene, CO_2, CO, hydrogen, etc.). Nitrogen was used as internal standard gas. Methane was used to normalize the concentration of products obtained by the two GCs.

For the extrapolated zero residence time experiments, 20–100 mg of samples were used and the dilution ratio by SiC was 25 to achieve reasonable bed length when very small amounts of catalysts were used. Keeping the reactant partial pressure and steam to carbon ratio, the overall flow rate was changed to get different residence time data.

Reactant conversion (Y_j) is defined as mole of reactants converted/mole of reactants fed. Product selectivity is defined per carbon basis as follows: (mole of $product_i$) × C_i/(mole of $reactants_j$ fed) × Y_j × C_j, where C_i and C_j are the carbon number in $product_i$ and $reactant_j$. Hydrogen selectivity was calculated as (mole of hydrogen per reacted reactant)/(theoretical mole of hydrogen per reacted reactants); the theoretical mole of hydrogen per reacted reactant is 6 for ethanol, 4 for acetaldehyde and 8 for acetone. The carbon balance calculated, based on the carbon out/carbon in, unless otherwise mentioned, was more than 95%.

2.4. Theoretical DFT calculations

The well-dispersed Co nanoparticles supported on the CNF are modeled using an optimized nanocluster (Co_{26}) containing 26 Co atoms with exposed (1 1 1) facets. The Co_{26} cluster interacting with acetone and ethanol in three-dimensional vacuum with side length of 20 Å were fully relaxed in the calculations. The spin-polarized PW91-generalized gradient approximation (GGA) functional [44] along with the projector augmented wave (PAW) pseudopotential [45] implemented in the Vienna ab initio simulation package (VASP) was used [46,47]. A plane wave basis set with kinetic cutoff energy of 400 eV and a (4 × 4 × 4) k-point sampling of the Brillouin zone were applied to reach the accuracy, i.e. the forces on all the atoms were less than 0.01 eV/Å. The adsorption energies of acetone and ethanol on the Co_{26} nanocluster were defined as

$$E_{ad} = E_{adsobate+Co\ cluster} - (E_{Co\ cluster} + E_{adsorbate}) \quad (1)$$

where $E_{Co\ cluster}$ is the total energy of the bare Co_{26} cluster, $E_{adsorbate}$ is the energy of the isolated adsorbate (acetone or ethanol) in the vacuum and $E_{adsorbate+Co\ cluster}$ is the total energy of one adsorbate interacting with the Co_{26} cluster. The negative value of E_{ad} indicates thermodynamically favorable.

3. Results and discussions

3.1. Characterization of catalysts

The BET surface areas of the obtained Co/ZrO_2 catalysts are summarized in Table 1. The surface area decreases slightly with the increase in cobalt loading. All the catalysts show comparable surface areas between 46 m^2/g and 58 m^2/g.

Cobalt loading has been widely used to prepare cobalt species with different reducibility [48]. We prepared Co–ZrO_2 catalysts of various cobalt loadings (i.e., 2 wt%, 5 wt% and 10 wt%) to obtain different Co^0/Co^{2+} ratios in an attempt to identify of possible active sites in the newly identified reaction pathway in ESR.

In situ XPS was used to confirm the tunable surface Co^0/Co^{2+} ratios of the catalysts. Fig. 1A shows the Co 2p XPS spectra of the as-synthesized Co–ZrO_2 catalysts. Based on both primary and satellite peak energies, Co^{2+} and Co^{3+} could be discerned by XPS [49]. Only Co^{2+} was observed on 2Co–ZrO_2. Co^{3+} was detected on 5Co–ZrO_2, and its fraction further increased on 10Co–ZrO_2. In line with this observation, XRD of 2Co–ZrO_2 does not show any diffraction of cobalt oxides, due to the highly dispersion of cobalt species. Whereas Co_3O_4 (3 1 1) diffraction was resolved on 5Co–ZrO_2, and the (3 1 1) peak was further intensified on 10Co–ZrO_2 (Fig. S1). It suggests that most of the cobalt species are Co^{2+} at lower cobalt loadings (e.g., 2 wt%), and those Co^{2+} possess strong interaction with ZrO_2 surface. At higher loading, cobalt species with weak metal–support interaction will form and increase with cobalt loading amounts, forming Co_3O_4 oxides (mixture of Co^{2+} and Co^{3+}). This can be further confirmed by the XPS characterization of the reduced samples.

Shown in Fig. 1B are the XPS spectra of in situ reduced catalysts, both Co^0 and Co^{2+} were detected on the reduced Co–ZrO_2

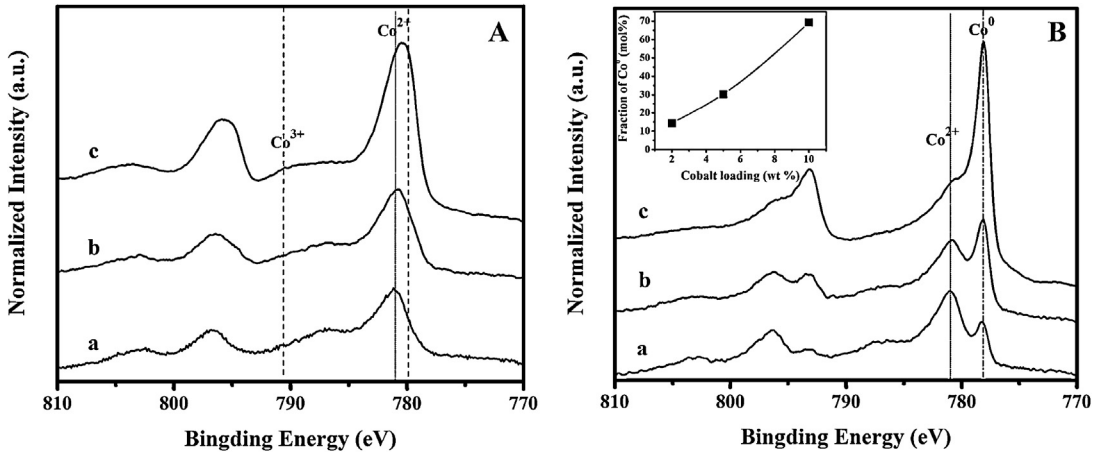

Fig. 1. In situ high-resolution Co 2p core-level spectra for (A) as-synthesized and (B) fresh Co–ZrO_2 catalysts (a: 2Co–ZrO_2, b: 5Co–ZrO_2, c: 10Co–ZrO_2). Inset in (B) is the mole fraction of Co^0 vs cobalt loading amounts.

catalysts. However, most of the cobalt on 2Co–ZrO_2 still retained its Co^{2+} oxidation state, which further confirms the strong interaction with ZrO_2. The fraction of Co^0 accounts for only ~14% of the overall surface cobalt species after reduction at 450 °C for 2 h. Upon increasing cobalt loading, all the Co^{3+} species detected in the as-synthesized samples disappeared, leaving only Co^0 and Co^{2+}, whereas the fraction of Co^0 increases, reaching ~30% on 5Co–ZrO_2 and 69% on 10Co–ZrO_2, respectively (inset in Fig. 1B). Notably, Co^{2+} species are always present on the Co–ZrO_2 catalysts reduced at 450 °C for 2 h. These results revealed that the strong interaction between cobalt and ZrO_2 suppresses the reduction of Co^{2+} species closely interacted with ZrO_2 support. Easy-to-reduce cobalt species could be manipulated with cobalt loading amounts to achieve variable Co^0/Co^{2+} ratios on Co–ZrO_2 catalysts.

H_2-TPR profiles were performed to further study the reducibility of the cobalt species on the Co–ZrO_2 catalysts. Due to the hydrogen spillover from cobalt to support [50], quantification was found hard to match the amount of reduced cobalt. However, consistent with the XPS results, the easy-to-reduce cobalt species increased significantly with the increase in cobalt loading, evidenced by the higher hydrogen consumption peak at low temperature (Fig. S2). In addition, it was also found that all the peaks shift to higher temperatures as the Co loading increases, the reason of which is unclear and could be related to the particles size of cobalt oxides.

3.2. Reaction pathway on Co–ZrO_2 catalysts

Time-on-stream experiments indicate that all the catalysts show an induction period of 1–2 h in which the activity and selectivity experience a rapid change. After the induction period, the catalyst becomes very stable and lasts for more than 30 h (Fig. S3) without showing any deactivation, and all the results shown below were measured after the induction period.

Over 10Co–ZrO_2 catalyst, the effect of residence time on the steady-state performance of ESR reaction is shown in Fig. 2. As the residence time decreases from 0.46 to 0.06 g. s. ml^{-1}, ethanol conversion decreases from 100% to 70%. Coincidently, the selectivities of acetone and acetaldehyde increase to ~40% and 7%, respectively. Meanwhile, the selectivity to CO_2 drops from 80% to 43%, indicating that both acetaldehyde and acetone are intermediates to CO_x. Only trace amounts of olefins were detected with the total selectivity less than 1% (not plotted in Fig. 2), and it is expected that these products were from the acidic-catalyzed dehydration side reactions, and its contribution is minor in the whole ESR reaction network. Separate experiments (Fig. S4) show that whether using ethanol or acetaldehyde or acetone as the starting reactant, the selectivities to the final products such as CO, CO_2 and CH_4 are similar under the same experimental condition over the 10Co–ZrO_2 catalyst. These experimental results further suggest that the ethanol steam reforming on Co/ZrO_2 go thorough acetaldehyde and acetone intermediates.

Ethanol dehydrogenation to acetaldehyde has been widely accepted as the first step in ESR (Eq. (I)), after which direct acetaldehyde steam reforming (Scheme 1, path 3) or acetaldehyde steam reforming via acetic acid intermediate (Scheme 1, path 1) has been proposed on most of the cobalt based catalysts [11,18]. Herein, our results clearly show the formation of another reaction intermediate (i.e., acetone). In addition, acetone steam reforming has been proved to be facile and selective to produce hydrogen on cobalt nanoparticles [33]. Other than the acetaldehyde steam reforming and acetic acid steam reforming proposed [18], acetone steam-reforming pathway should also be expected on the 10Co–ZrO_2 catalyst. Consistent with our observation, by using ethanol temperature-programmed desorption experiments, Benito [38] and Song et al. [11,12] also reported acetone formation and acetone steam reforming at elevated temperatures (>500 °C) on the Co–La/ZrO_2 and Co/ZrO_2 catalysts, respectively. It should be mentioned that although ethanol-to-acetone conversion has been widely accepted on (modified) ZrO_2 metal oxides via a condensation/ketonization pathway [8,11,12,26,37,43,51,52], there is no

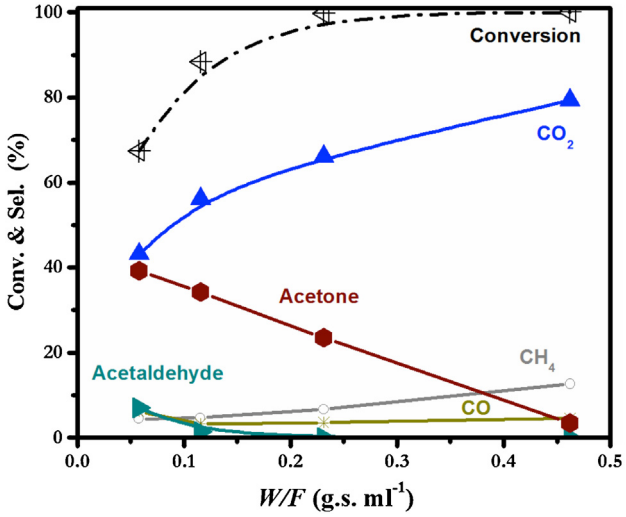

Fig. 2. Dependence of activity and products selectivity on the residence time during the steady-state ethanol steam reforming on 10Co–ZrO_2 (100 mg, 7.2 kPa ethanol, 72 kPa H_2O, T = 450 °C, N_2 was used as dilution gas).

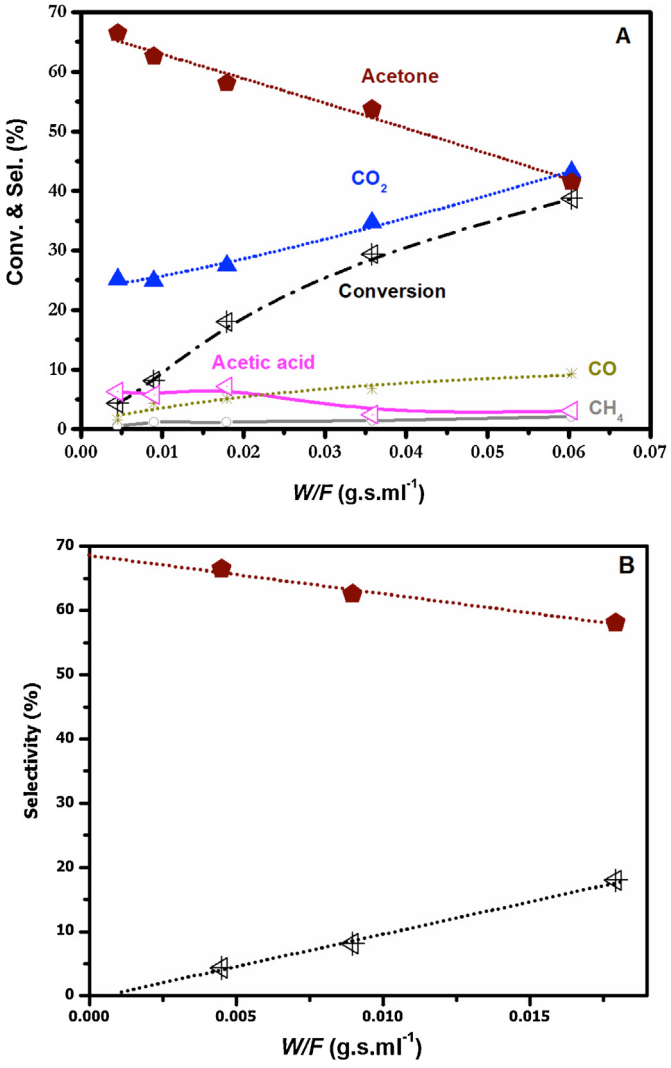

Fig. 3. Dependence of product selectivity on the residence time during the acetaldehyde steam reforming on the 10Co–ZrO_2 catalyst (A); maximum selectivity to acetone intermediate at extrapolated zero residence time (B) (10–20 mg, 7.2 kPa acetaldehyde, 72 kPa H_2O, T = 450 °C, N_2 was used as dilution gas).

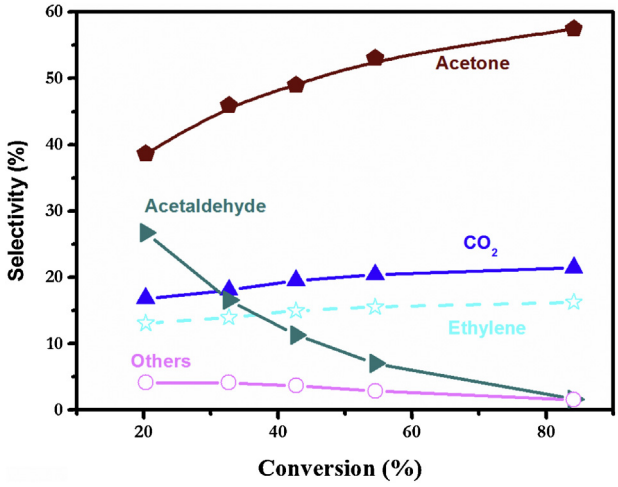

Fig. 4. Product evolution as a function of ethanol conversions on 2Co–ZrO_2 (50 mg catalyst, W/F = 0.01–0.12 g.s.ml^{-1}, 7.2 kPa ethanol, 72 kPa H_2O, T = 450 °C). Others represent mainly acetic acid, propylene and isobutene.

report quantitatively addressing the role of acetone steam reforming (Scheme 1, path 2) in ESR on Co–ZrO_2 catalysts. From Fig. 2, a favorable acetaldehyde-to-acetone reaction kinetics against acetone steam reforming was evidenced by the much higher acetone selectivity than acetaldehyde one (40% vs 7%) at low residence time. Herein, zero residence time extrapolation experiments [53], using acetaldehyde/H_2O (S/C = 5) as reactant (acetaldehyde steam reforming), were performed to determine the role that the new pathway (Scheme 1, path 2) plays in ESR on the 10Co–ZrO_2 catalysts. Assuming ESR occurs via acetone pathway on 10Co–ZrO_2 (Scheme 1, path 2), ~75% acetone selectivity can be expected (per the stoichiometry of Eqs. (II)–(IV)) at extrapolated zero residence time since acetone steam reforming is the limit step.

$$CH_3CH_2OH \rightarrow CH_3CHO + H_2 \quad (I)$$

$$CH_3CHO + H_2O \rightarrow CH_3COOH + H_2 \quad (II)$$

$$2CH_3COOH \rightarrow CH_3COCH_3 + CO_2 + H_2O \quad (III)$$

$$2CH_3CHO + H_2O \rightarrow CH_3COCH_3 + CO_2 + H_2 \quad (IV)$$

As expected, acetone selectivity decreases with increasing residence time as a result of the steam reforming to CO_2 and hydrogen, as shown in Fig. 3A. At extrapolated zero residence time (Fig. 3B), the selectivity to acetone reaches approximately 69%, while the CO and CO_2 selectivities are only about 3% and 22%. Two possible routes (i.e., ketonization of acetic acid and condensation of acetaldehyde) had been proposed for acetaldehyde-to-acetone conversion [51]. In the first route, acetaldehyde is oxidized to acetic acid in the presence of oxygen or water (Eq. (II)), and then acetic acid ketonization (Eq. (III)) to acetone. From current experiments, acetic acid was indeed observed with highest selectivity being ~6% and decreased as residence time increased (Fig. 3). However, given the low acetic acid selectivity, predominant ketonization of acetic acid could not be excluded for the possible faster kinetics of ketonization than that of acetaldehyde-to-acetic acids. The second acetone formation route is acetaldehyde condensation that was also proposed on other supported (e.g., CeO_2, ZnO and $Zn_xZr_yO_z$) catalysts during the ethanol steam-reforming reaction [8,12,18,43].

As aforementioned, a maximum theoretical selectivity of 75% can be expected for acetone in the acetaldehyde-to-acetone conversion. Our experimental selectivity to acetone at extrapolated zero residence time is ~69% along with ~6% acetic acid, which is close to its theoretical selectivity. It suggests that formation of acetone followed by acetone steam reforming (Scheme 1, path 2) is a major reaction pathway (>90%) on 10Co–ZrO_2 catalysts during ESR. Direct steam reforming of acetaldehyde (Scheme 1, path 3) is minor, and acetic acid steam reforming could contribute but play a smaller role (<6%).

To summarize this part, the major (>90% of carbon) reaction pathway from ethanol to acetaldehyde and to acetone and then to steam-reforming products (Scheme 1, black highlighted pathway) has been identified in ESR on the 10Co–ZrO_2 catalysts.

3.3. Active sites

A major reaction pathway for ethanol steam reforming was identified on the 10Co–ZrO_2 catalyst. In this new reaction pathway, ethanol was first dehydrogenated to acetaldehyde which was then converted into acetone via a condensation/ketonization process. The acetone produced was further steam reformed to CO_x and hydrogen (Scheme 1, black highlighted pathway). The possible active sites in the new reaction pathway were further studied and discussed.

On the pure ZrO_2 support, acid-catalyzed dehydration was the dominant reaction in the ESR, forming mainly ethylene (>90%, data not shown here), consistent with our previous report [43]. With the

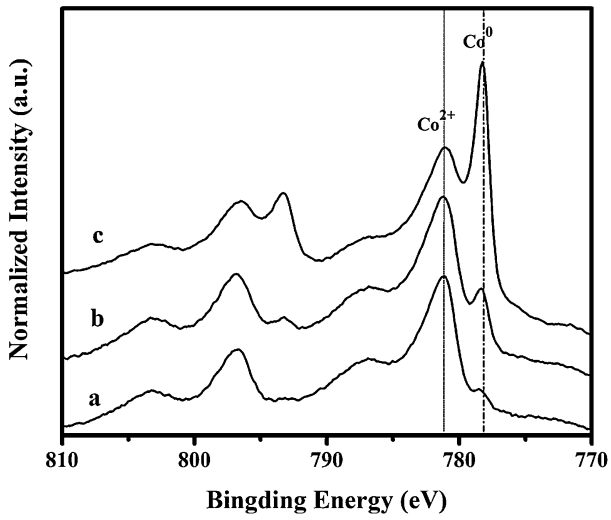

Fig. 5. In situ high-resolution Co 2p core-level spectra for reduced (a) 2 wt% Co/ZrO_2, (b) 5 wt% Co/ZrO_2, (c) 10 wt% Co/ZrO_2, and then exposed to 3% H_2O in helium at 450 °C for 30 min.

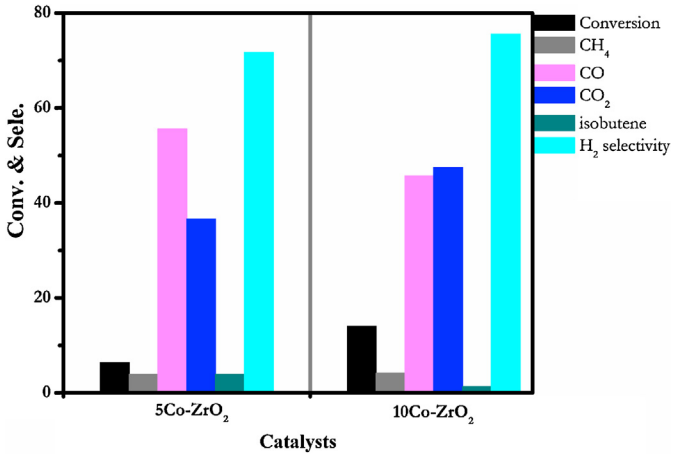

Fig. 6. Performance of acetone steam-reforming reactions on $Co–ZrO_2$ catalysts with different cobalt loadings. (50–100 mg catalyst, $W/F = 0.008$ g. s. ml^{-1}, 4.7 kPa acetone, 70.5 kPa H_2O, $T = 450$ °C. Carbon balance is more than 90%.)

introduction of small amounts of cobalt (2 wt%), ethylene selectivity decreased significantly to be less than 20% on $2Co–ZrO_2$ (Fig. 4). Meanwhile, substantial amounts of acetone and CO_x (mostly CO_2) were observed, along with the formation of small amounts of methane and isobutene (<1%). It suggests that the addition of cobalt suppresses the dehydration and enhances the dehydrogenation reaction pathway. Indeed, oxidized cobalt (i.e., Co^{2+}) has been demonstrated to be highly active for ethanol dehydrogenation to acetaldehyde [32,54]. The formation of isobutene is related to the acid–base-catalyzed secondary acetone condensations [43]. Noteworthy, selectivities to acetone and CO_2 increase with ethanol conversions (i.e., longer residence time) at the expense of acetaldehyde and acetic acid, confirming that acetone is indeed produced from the secondary condensation/ketonization of acetaldehyde [34,51]. Most importantly, acetone selectivity on $2Co–ZrO_2$ barely shows correlations with the steam-reforming products (e.g., H_2, CO_x) over a wide range of ethanol conversions from ~20% to ~84% (Fig. 4). On the other hand, acetone selectivity on $10Co–ZrO_2$ decreases with the concurrent formation of steam-reforming products as the ethanol conversion increases (Fig. 2). At a similar ethanol conversion (88% vs 84%), the acetone selectivity is ~34% on $10Co–ZrO_2$ and ~57% on $2Co–ZrO_2$, while the selectivities to steam-reforming products (i.e., H_2 and CO_x) show the opposite trend (Fig. S5). These results reveal that the $2Co–ZrO_2$ catalyst bears the active sites for ethanol conversion to acetone, however, lacks those for further acetone steam-reforming reactions.

We have shown that metallic cobalt nanoparticles are highly active and selective for acetone steam reforming to CO_2 and H_2 [33]. Herein, from XPS, the fraction of Co^0 (or Co^0/Co^{2+} ratio) increased with cobalt loading amounts (Table 1), and the absolute Co^0 amounts increased accordingly. Consistent with this trend, enhanced acetone steam-reforming reactions were also observed (Fig. S5). It further confirmed that Co^0 is the active sites for acetone steam reforming [33].

It should be noted that a small amount of Co^0 was observed on fresh $2Co–ZrO_2$ catalyst (Table 1), whereas no obvious acetone steam reforming was detected. It has been reported that the cobalt oxidation state of the catalyst is determined by the composition of reaction stream [14]. Especially, the presence of water in the reactant will re-oxidize the metallic cobalt formed during the pretreatment [31]. We further studied the cobalt oxidation state of the $Co–ZrO_2$ catalysts in the presence of water (Fig. 5), using XPS. The fractions of Co^0 are summarized in Table 1. It is clear that, upon exposing the catalyst to H_2O, although the trend of the fraction of Co^0 is still same and increases with cobalt loading amounts, the fraction of Co^0 decreases significantly to 1.4% on $2Co–ZrO_2$, 9% on $5Co–ZrO_2$ and 40% on $10Co–ZrO_2$, respectively (Table 1). These results confirm that most of the Co^0 on the fresh $2Co–ZrO_2$ is indeed re-oxidized in the presence of water, possibly leading to the non-observable acetone steam-reforming activity.

To further confirm this, separate experiments using acetone as reactant (i.e., acetone steam reforming) were also performed on the $Co–ZrO_2$ catalysts. As expected, no steam-reforming products (i.e., H_2, CO_x and CH_4) were observed on $2Co–ZrO_2$. While acetone steam-reforming reactions were obvious on $5Co–ZrO_2$ and $10Co–ZrO_2$, higher acetone conversion (14.0%) was achieved on $10Co–ZrO_2$ than on $5Co–ZrO_2$ (6.4%) at the same reaction conditions (Fig. 6), in agreement with our XPS observation (Table 1). In addition, water gas shift reaction is more efficient on $10Co–ZrO_2$, evidenced by its high CO_2 selectivity and high H_2 yield, consistent with the observation that the metallic cobalt is the active site for water gas shift reactions [16]. The fact that no observable steam reforming was observed on $2Co–ZrO_2$ is mainly due to the re-oxidation of Co^0 as verified by our in situ XPS observation. However, ZrO_2 support-catalyzed acetone polymerization/coking of the small fraction of Co^0 cannot be excluded. Consistent with the ESR results (Fig. 4), no Co^0 seems to be present under the acetone steam-reforming conditions on $2Co–ZrO_2$.

Regarding the ethanol-to-acetone conversion [8,11,12,26,37,43,51,52], a balanced surface acid–base is essential to ethanol dehydrogenation (versus dehydration) to acetaldehyde followed by the acetaldehyde condensation/ketonization to acetone [26,43]. Despite the fact that both acid and base are present on ZrO_2 [55], ethylene is mainly produced, suggesting the surface acidity plays the major role for ethanol dehydration reaction. Upon the introduction of Co (i.e., $2Co–ZrO_2$), the dehydration reaction is largely suppressed and dehydrogenation and condensation/ketonization to acetone is significantly enhanced (Fig. 4). Similar to ZnO, it is proposed that CoO closely interacted with ZrO_2 support could passivate the surface acidity and enhance the ethanol dehydrogenation activity [54]. The balanced acid–base properties play a pivotal role in the following acetaldehyde condensation/ketonization reactions toward acetone [26].

To summarize this part, Co^0 acts as the active site for the acetone steam-reforming reactions during ESR on the $Co–ZrO_2$. A small amount of cobalt species can modify the surface chemistry of ZrO_2, suppressing dehydration and promoting dehydrogenation/condensation of ethanol to acetone. However, at current

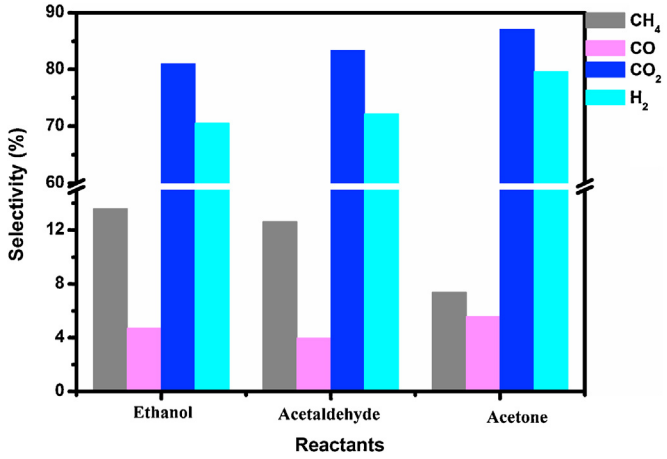

Fig. 7. Dependence of products selectivity on the initial reactants during the steam reforming on 8Co-CNF. (100 mg, $W/F = 0.12$ g. s. ml^{-1}, ~3.6 kPa C, 18.0 kPa H_2O, $T = 450$ °C, conversion at 100%.)

reaction conditions, higher cobalt loading (>5 wt%) seems pivotal to maintain enough active sites (i.e., metallic cobalt) for further conversion of the formed acetone intermediate to final steam-reformed products.

3.4. Evolution of catalyst structure and the functionality

To further explore the structure–performance of the Co–ZrO_2 catalysts in ESR, the morphological structure of the working catalysts was also investigated. Catalyst that is still functioning in ESR was cooled down under nitrogen flow and collected for TEM characterization. It was found that, after the induction period, all the spent catalysts except for 2Co–ZrO_2 (Fig. S6A) suffered a structural change during ESR, where cobalt nanoparticles initially sitting on ZrO_2 support were separated from the support to form the Co/CNF/ZrO_2 structure where metallic cobalt nanoparticles are sitting at the tip of CNF (Fig. S6B and C). The lack of Co/CNF over spent 2Co-ZrO_2 further confirms its absence of metallic cobalt particles. In contrast, the presence of metallic cobalt particles on the 5Co-ZrO_2 and 10Co-ZrO_2 working catalyst, as confirmed by XPS, leads to the formation of Co/CNF/ZrO_2 structure. Despite the mixed results that filament carbon leads to [20] or mitigate [56,57] the deactivation of cobalt catalysts, it is reported that the catalysts with Co/CNF structure are still active in ESR [56,57]. The formed Co/CNF, similar to Co/g-AC [33], play the key role in the steam reforming of acetone intermediate. Herein, to investigate how the developed Co/CNF/ZrO_2 structure works in the formation and steam reforming of acetone intermediate, 8Co-CNF was prepared for the steam-reforming experiment. Given the inert nature, carbon-supported cobalt (i.e., Co/g-AC) is highly resistant to oxidation by water (Fig. S7), indicating that cobalt on 8Co-CNF or Co/CNF maintains in metallic form (Co^0) under reaction conditions. For ESR, only acetaldehyde (no acetone) was observed in the liquid product irrespective of ethanol conversions (data not shown), which matches well with those on Co/g-AC [33]. It is thus concluded that acetone formation is closely related to the modified Co^{2+}–ZrO_2 support with balanced acid–base properties, evidenced by our aforementioned discussions (Section 3.3). Moreover, both ESR and acetaldehyde steam reforming on 8Co-CNF showed methane selectivity twice higher than that of 10Co–ZrO_2 (~14% vs ~6%) under same reaction conditions, while acetone steam reforming on 8Co-CNF gave methane selectivity close to that of ESR on 10Co–ZrO_2 (~6%; Fig. 7). These results suggest that the low methane selectivity in ESR over Co/CNF/ZrO_2 was not a result of direct ethanol reaction on Co/CNF, but instead, due to ethanol conversion on the support to first produce acetone, and

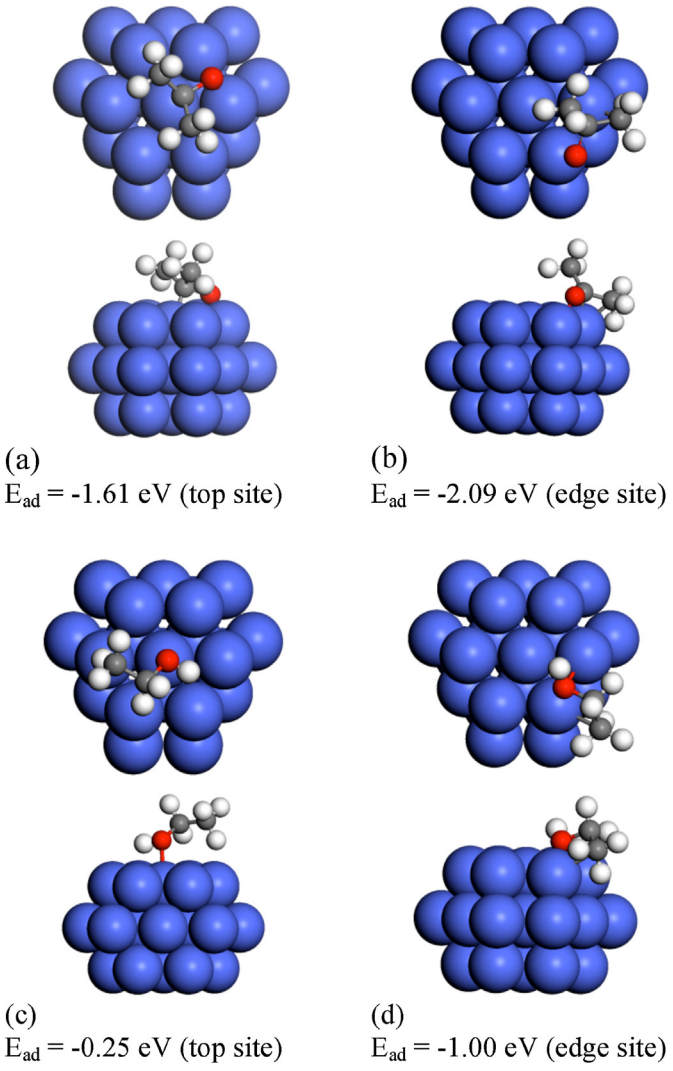

Fig. 8. Acetone and ethanol adsorption on the Co nanoparticles. (a) Acetone on the top site; (b) acetone on the edge (corner) site; (c) ethanol on the top site; (d) ethanol on the edge (corner) site.

then the acetone steam reforming over Co/CNF (Scheme S1), on which Co^0 are dominant (Fig. S7). This also further confirms the major reaction pathway and active sites proposed in Sections 3.2 and 3.3.

While it is still unclear why ethanol selectively reacts on Co^{2+}–ZrO_2 support to form acetone intermediate which then transfers to the cobalt nanoparticles for acetone steam-reforming reactions, our theoretical DFT calculations suggest that adsorption energies of ethanol and acetone on metallic cobalt nanoparticle are significantly different. On both top and edge sites of the Co nanoparticle, the acetone adsorption is much stronger than the ethanol adsorption (Fig. 8). Therefore, we can hypothesize that the strongly bonding acetone species which is produced in the steady-state ESR reaction will prevent the ethanol adsorption and reaction on the Co/CNF.

4. Conclusions

We identified a new ESR reaction pathway on the Co–ZrO_2 catalysts. In this reaction pathway, ethanol was firstly dehydrogenated to form acetaldehyde, which was then converted into acetone via a condensation/ketonization process. The formed acetone was further steam reformed to produce hydrogen, CO_x and small amounts

of CH_4 products. More than 90% of carbon was found to follow this reaction pathway. During the ESR, catalyst structure will self-develop into a special Co/CNF/ZrO_2 structure, on which ethanol conversion to acetone was mainly achieved on the acid–base sites of the Co^{2+}–ZrO_2 support, and acetone steam reforming occurred on Co/CNF. This work not only provides insights into the reaction mechanisms of ESR on Co–ZrO_2 catalysts, but also provides guidances to develop a new high selective H_2 product process by steam reforming of acetone. For example, a two-step reaction process can be designed: ethanol is first selectively converted into acetone on metal oxides [43,51] and then acetone steam reforming on an inert (e.g., carbon)-supported cobalt nanoparticles [33].

Acknowledgements

We gratefully acknowledge financial support from the U.S. Department of Energy (DOE), Office of Basic Energy Sciences, Division of Chemical Sciences, Geosciences, and Biosciences. The EMSL is a U.S. DOE national scientific user facility located at PNNL and sponsored by the U.S. DOE's Office of Biological and Environmental Research.

Appendix A. Supplementary data

Supplementary data associated with this article can be found, in the online version, at http://dx.doi.org/10.1016/j.apcatb.2014.06.043.

References

[1] R.D. Cortright, R.R. Davda, J.A. Dumesic, Nature 418 (2002) 964–967.
[2] F. Haga, T. Nakajima, H. Miya, S. Mishima, Catal. Lett. 48 (1997) 223–227.
[3] F. Frusteri, S. Freni, L. Spadaro, V. Chiodo, G. Bonura, S. Donato, S. Cavallaro, Catal. Commun. 5 (2004) 611–615.
[4] M.S. Batista, R.K.S. Santos, E.M. Assaf, J.M. Assaf, E.A. Ticianelli, J. Power Sources 124 (2003) 99–103.
[5] A. Kaddouri, C. Mazzocchia, Catal. Commun. 5 (2004) 339–345.
[6] J. Llorca, N. Homs, J. Sales, J.L.G. Fierro, P.R. de la Piscina, J. Catal. 222 (2004) 470–480.
[7] J. Llorca, N. Homs, J. Sales, P.R. de la Piscina, J. Catal. 209 (2002) 306–317.
[8] B.C. Zhang, X.L. Tang, Y. Li, W.J. Cai, Y.D. Xu, W.J. Shen, Catal. Commun. 7 (2006) 367–372.
[9] H. Song, L.Z. Zhang, U.S. Ozkan, Green Chem. 9 (2007) 686–694.
[10] H. Song, L.Z. Zhang, R.B. Watson, D. Braden, U.S. Ozkan, Catal. Today 129 (2007) 346–354.
[11] H. Song, X.G. Bao, C.M. Hadad, U.S. Ozkan, Catal. Lett. 141 (2011) 43–54.
[12] H. Song, U.S. Ozkan, J. Catal. 261 (2009) 66–74.
[13] H. Song, L.Z. Zhang, U.S. Ozkan, Ind. Eng. Chem. Res. 49 (2010) 8984–8989.
[14] S.S.Y. Lin, D.H. Kim, M.H. Engelhard, S.Y. Ha, J. Catal. 273 (2010) 229–235.
[15] S.S.Y. Lin, D.H. Kim, S.Y. Ha, Catal. Lett. 122 (2008) 295–301.
[16] A.M. Karim, Y. Su, M.H. Engelhard, D.L. King, Y. Wang, ACS Catal. 1 (2011) 279–286.
[17] A.M. Karim, Y. Su, J.M. Sun, C. Yang, J.J. Strohm, D.L. King, Y. Wang, Appl. Catal. B 96 (2010) 441–448.
[18] J. Llorca, N. Homs, P.R. de la Piscina, J. Catal. 227 (2004) 556–560.
[19] C.X. Zhang, H.R. Yue, Z.Q. Huang, S.R. Li, G.W. Wu, X.B. Ma, J.L. Gong, ACS Sustain. Chem. Eng. 1 (2013) 161–173.
[20] J.C. Vargas, S. Libs, A.C. Roger, A. Kiennemann, Catal. Today 107–108 (2005) 417–425.
[21] C.X. Zhang, W.C. Zhu, S.R. Li, G.W. Wu, X.B. Ma, X. Wang, J.L. Gong, Chem. Commun. 49 (2013) 9383–9385.
[22] A. Haryanto, S. Fernando, N. Murali, S. Adhikari, Energy Fuels 19 (2005) 2098–2106.
[23] P.D. Vaidya, A.E. Rodrigues, Chem. Eng. J. 117 (2006) 39–49.
[24] M. Ni, D.Y.C. Leung, M.K.H. Leung, Int. J. Hydrogen Energy 32 (2007) 3238–3247.
[25] L.V. Mattos, G. Jacobs, B.H. Davis, F.B. Noronha, Chem. Rev. 112 (2012) 4094–4123.
[26] J. Sun, Y. Wang, ACS Catal. 4 (2014) 1078–1090.
[27] Z.H. Wei, J.M. Sun, Y. Li, A.K. Datye, Y. Wang, Chem. Soc. Rev. 41 (2012) 7994–8008.
[28] S.D. Davidson, H. Zhang, J. Sun, Y. Wang, Dalton Trans. (2014), http://dx.doi.org/10.1039/C1034DT00521J.
[29] P.O. Graf, D.J.M. de Vlieger, B.L. Mojet, L. Lefferts, J. Catal. 262 (2009) 181–187.
[30] S. Davidson, J. Sun, Y. Wang, Top. Catal. 56 (2013) 1651–1659.
[31] V.M. Lebarbier, A.M. Karim, M.H. Engelhard, Y. Wu, B.Q. Xu, E.J. Petersen, A.K. Datye, Y. Wang, ChemSusChem 4 (2011) 1679–1684.
[32] S.D. Davidson, J. Sun, Y. Hong, A.M. Karim, A.K. Datye, Y. Wang, Catal. Today 233 (2014) 38–45.
[33] J.M. Sun, D.H. Mei, A.M. Karim, A.K. Datye, Y. Wang, ChemCatChem 5 (2013) 1299–1303.
[34] K. Takanabe, K. Aika, K. Inazu, T. Baba, K. Seshan, L. Lefferts, J. Catal. 243 (2006) 263–269.
[35] K. Takanabe, K. Aika, K. Seshan, L. Lefferts, Chem. Eng. J. 120 (2006) 133–137.
[36] M.P. Hyman, J.M. Vohs, Surf. Sci. 605 (2011) 383–389.
[37] M. Benito, R. Padilla, A. Serrano-Lotina, L. Rodriguez, J.J. Brey, L. Daza, J. Power Sources 192 (2009) 158–164.
[38] J.Y.Z. Chiou, J.Y. Siang, S.Y. Yang, K.F. Ho, C.L. Lee, C.T. Yeh, C.B. Wang, Int. J. Hydrogen Energy 37 (2012) 13667–13673.
[39] L. Garcia, R. French, S. Czernik, E. Chornet, Appl. Catal. A 201 (2000) 225–239.
[40] X. Hu, G.X. Lu, Appl. Catal. B 88 (2009) 376–385.
[41] M.I. Zaki, M.A. Hasan, L. Pasupulety, Langmuir 17 (2001) 768–774.
[42] W. Chen, X.L. Pan, M.G. Willinger, D.S. Su, X.H. Bao, J. Am. Chem. Soc. 128 (2006) 3136–3137.
[43] J.M. Sun, K.K. Zhu, F. Gao, C.M. Wang, J. Liu, C.H.F. Peden, Y. Wang, J. Am. Chem. Soc. 133 (2011) 11096–11099.
[44] J.P. Perdew, K. Burke, M. Ernzerhof, Phys. Rev. Lett. 77 (1996) 3865–3868.
[45] G. Kresse, D. Joubert, Phys. Rev. B 59 (1999) 1758–1775.
[46] G. Kresse, J. Furthmuller, Comput. Mater. Sci. 6 (1996) 15–50.
[47] G. Kresse, J. Hafner, Phys. Rev. B 48 (1993) 13115–13118.
[48] W.J. Wang, Y.W. Chen, Appl. Catal. 77 (1991) 223–233.
[49] S.A. Chambers, R.F.C. Farrow, S. Maat, M.F. Toney, L. Folks, J.G. Catalano, T.P. Trainor, G.E. Brown, J. Magn. Magn. Mater. 246 (2002) 124–139.
[50] D.I. Enache, M. Roy-Auberger, R. Revel, Appl. Catal. A 268 (2004) 51–60.
[51] R.S. Murthy, P. Patnaik, P. Sidheswaran, M. Jayamani, J. Catal. 109 (1988) 298–302.
[52] C. Liu, A. Karim, V. Lebarbier, D. Mei, Y. Wang, Top. Catal. 56 (2013) 1782–1789.
[53] K. Chen, S. Xie, A.T. Bell, E. Iglesia, J. Catal. 198 (2001) 232–242.
[54] E. Martono, M.P. Hyman, J.M. Vohs, Phys. Chem. Chem. Phys. 13 (2011) 9880–9886.
[55] K. Tanabe, T. Yamaguchi, Catal. Today 20 (1994) 185–198.
[56] H. Wang, Y. Liu, L. Wang, Y.N. Qin, Chem. Eng. J. 145 (2008) 25–31.
[57] A.L. Alberton, M. Souza, M. Schmal, Catal. Today 123 (2007) 257–264.